SCIENCE CHINA
Chemistry

•ARTICLES•

May 2018 Vol.61 No.5: 531–537
https://doi.org/10.1007/s11426-017-9199-1

Synergistic effect of fluorination on both donor and acceptor materials for high performance non-fullerene polymer solar cells with 13.5% efficiency

Qunping Fan[1], Wenyan Su[1], Yan Wang[1], Bing Guo[1], Yufeng Jiang[3], Xia Guo[1], Feng Liu[2], Thomas P. Russell[3], Maojie Zhang[1*] & Yongfang Li[1,4]

[1]*State and Local Joint Engineering Laboratory for Novel Functional Polymeric Materials, Laboratory of Advanced Optoelectronic Materials, College of Chemistry, Chemical Engineering and Materials Science, Soochow University, Suzhou 215123, China;*
[2]*Department of Physics and Astronomy, Collaborative Innovation Center of IFSA, Shanghai Jiao Tong University, Shanghai 200240, China;*
[3]*Materials Sciences Division, Lawrence Berkeley National Laboratory, Berkeley, California 94720, United States;*
[4]*CAS Research/Education Center for Excellence in Molecular Sciences, CAS Key Laboratory of Organic Solids, Institute of Chemistry, Chinese Academy of Sciences, Beijing 100190, China*

Received December 18, 2017; accepted December 21, 2017; published online January 24, 2018

A high performance polymer solar cells (PSCs) based on polymer donor PM6 containing fluorinated thienyl benzodithiophene unit and *n*-type organic semiconductor acceptor IT-4F containing fluorinated end-groups were developed. In addition to complementary absorption spectra (300–830 nm) with IT-4F, the PM6 also has a deep HOMO (the highest occupied molecular) level (−5.50 eV), which will lower the open-circuit voltage (V_{oc}) sacrifice and reduce the E_{loss} of the IT-4F-based PSCs. Moreover, the strong crystallinity of PM6 is beneficial to form favorable blend morphology and hence to suppress recombination. As a result, in comparison with the PSCs based on a non-fluorinated D/A pair of PBDB-T:ITIC with a medium PCE of 11.2%, the PM6:IT-4F-based PSCs yielded an impressive PCE of 13.5% due to the synergistic effect of fluorination on both donor and acceptor, which is among the highest values recorded in the literatures for PSCs to date. Furthermore, a PCE of 12.2% was remained with the active layer thickness of up to 285 nm and a high PCE of 11.4% was also obtained with a large device area of 1 cm^2. In addition, the devices also showed good storage, thermal and illumination stabilities with respect to the efficiency. These results indicate that fluorination is an effective strategy to improve the photovoltaic performance of materials, as well as the both fluorinated donor and acceptor pair-PM6:IT-4F is an ideal candidate for the large scale roll-to-roll production of efficient PSCs in the future.

polymer solar cells, fluorine substitution, non-fullerene, wide bandgap conjugated polymer, power conversion efficiency

Citation: Fan Q, Su W, Wang Y, Guo B, Jiang Y, Guo X, Liu F, Russell TP, Zhang M, Li Y. Synergistic effect of fluorination on both donor and acceptor materials for high performance non-fullerene polymer solar cells with 13.5% efficiency. *Sci China Chem*, 2018, 61: 531–537, https://doi.org/10.1007/s11426-017-9199-1

1 Introduction

In the last three years, the polymer solar cells (PSCs) based on *n*-type organic semiconductor (*n*-OS) acceptor have become the focus of attention [1–13] and made great progress with the power conversion efficiencies (PCEs) of up to 11%–14% to date [14–30]. Recently, small bandgap *n*-OS acceptors based on a fused-ring electron-donating core along with two strong electron-withdrawing end-groups (such as IDIC, ITIC and IT-M) have become dominate in high efficiency PSCs [28,31,32]. In comparison with the traditional fullerene derivatives, these *n*-OS acceptors show easily adjustable

*Corresponding author (email: mjzhang@suda.edu.cn)

absorption spectrum, molecular energy levels, and charge mobility by the simple chemical structure modification [31–39].

Recently, fluorine atom has been widely introduced into organic semiconductor materials to synergistically improve the molecular energy levels, optical absorption and carrier mobility properties for photovoltaic applications, resulting from its maximum electronegativity in the periodic table and small atomic radius [18,23,40,41]. In addition, fluorination as a simple and effective molecular modification strategy was also used to optimize the active layer morphology due to the enhancement of crystallinity of the resulting molecules, which eventually improves the PCE of PSCs [42–51]. For example, Hou *et al*. [26] reported an high-performance fluorinated *n*-OS acceptor, IT-4F, by introducing fluorine (F) atoms to end-groups (Figure S1 and Table S1, Supporting Information online). Compared with the non-fluorinated counterparts ITIC [31], IT-4F showed a reduced optical bandgap and decreased molecular energy levels due to the strong electron-withdrawing ability of F atom, which enhanced the electronic push-pull effect between the DTIDT donor core and the EG-2F acceptor end-groups. Moreover, fluorination also enhanced intermolecular interactions through non-covalent interactions (C–F···H, C–F···S and C–F···π), which improved the crystallinity and hence facilitate to achieve higher absorption coefficient and electron mobility [18,52–57]. As a result, the IT-4F-based PSCs showed a PCE of 13.1% with a high short circuit current density (J_{sc}) of 20.5 mA cm^{-2} and fill factor (FF) of 71.9% [26]. Meanwhile, Zhan *et al*. [18] also reported a series of fluorinated *n*-OS acceptors (Figure S1 and Table S1) and found that the acceptors showed broaden and enhanced absorption, and improved electron mobility with increasing F atom on end-capping groups IC. Finally, the PSCs based on the tetra-fluorinated acceptor INIC3 showed a high PCE of 11.5%. Notably, the other PSCs based on *n*-OS acceptors with fluorinated end-group also show the similar phenomena with improved device performance [34,58].

The well-matched pair of polymer donor and *n*-OS acceptor plays a key role in achieving high efficiency PSCs. Extensive research has proved that fine-tuning structure of polymer donor through fluorine substitution could effectively improve the material characteristics and hence promote the PCEs of PSCs [40–55]. Our previous work [41] has reported a fluorinated-thienyl benzodithiophene (BDT-2F)-based donor polymer PM6 (Figure 1(a)). Compared with the non-fluorinated counterpart PBDB-T [59], PM6 showed decreased molecular energy levels, improved absorption coefficient with a similar optical bandgap, stronger intermolecular π-π stacking interactions and increased crystallinity. With the small bandgap *n*-OS ITIC as acceptor, the PM6:ITIC blend film showed a broad and strong absorption spectrum from 300–780 nm. However, the PSCs based on PM6:ITIC only achieved a moderate PCE of 9.7% with relatively lower J_{sc} and FF, despite of a high open-circuit voltage (V_{oc}) of up to 1.04 V [60]. Hence, in order to further improve the photovoltaic performance of this PM6:ITIC-based PSCs, it should be a simple and feasible strategy to choose IT-4F as acceptor, which can enhance the light harvesting, increase the ΔE_{HOMO} ($HOMO_{donor}$–$HOMO_{acceptor}$; HOMO is the highest occupied molecular) between the donor and acceptor and optimize the blend morphology for higher J_{sc} and FF.

Therefore, in this work, we fabricated the PSCs based on PM6 as donor and IT-4F as acceptor and investigated the photovoltaic performance of the devices. The PM6:IT-4F pair showed a broader and more complementary absorption spectra from 300 to 830 nm (Figure 1(b)) in comparison with the PBDB-T:ITIC blend, and displayed a larger ΔE_{HOMO} of 0.19 eV vs. 0.1 eV for PM6:ITIC blend (Figure 1(c)), which would facilitate to obtain a higher J_{sc} in devices. Furthermore, the ΔE_{LUMO} ($LUMO_{donor}$–$LUMO_{acceptor}$; LUMO is the lowest unoccupied molecular orbital) in PM6:IT-4F pair is 0.46 eV (Figure 1(c)), which provides a powerful driving force for the charge separation at the bulk interface. In addition, the strong crystallinity of PM6 is beneficial to form favorable blend morphology and hence to suppress recombination in devices. Therefore, in comparison with the PSCs based on a non-fluorinated D/A pair of PBDB-T:ITIC with a medium PCE of 11.2% [22], the PM6:IT-4F-based

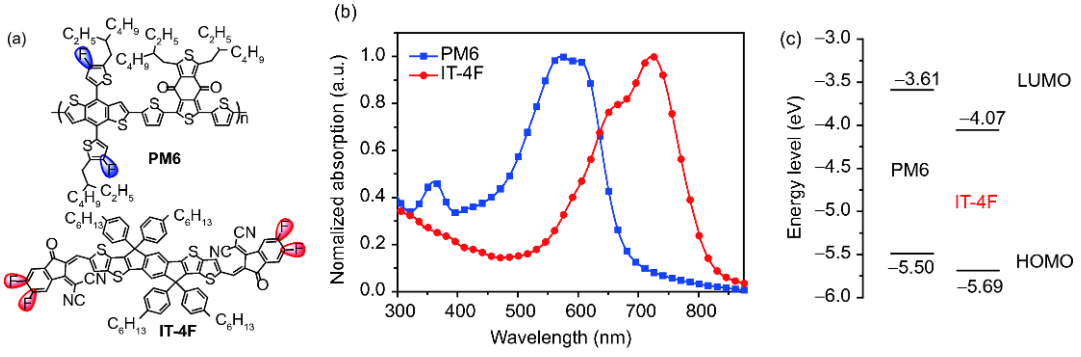

Figure 1 (a) Molecular structures, (b) UV-Vis absorption spectra in films and (c) molecular energy level diagrams of PM6 and IT-4F (color online).

PSCs achieved a higher PCE of 13.5% with a V_{oc} of 0.84 V, J_{sc} of 22.2 mA cm^{-2} and FF of 72.5% due to the synergistic effect of fluorination on both donor and acceptor. To the best of our knowledge, the PCE of 13.5% is among the highest values recorded in the literature for PSCs to date.

2 Results and discussion

The devices with a structure of ITO/ZnO/PFN/PM6:IT-4F/MoO_3/Al were fabricated to probe the photovoltaic properties of PSCs, and the detailed preparation processes are recorded in the Supporting Information online. The current-voltage (*J-V*) characteristics of the PSCs are shown in Figure S2 and detailed photovoltaic parameters are summarized in Table S2. For the D/A (PM6:IT-4F) weight ratios from 1.5:1 to 1:1.5 as shown in Figure S2(a), all the devices show PCEs over 10% with high V_{oc} of 0.89–0.90 V, and the optimal PCE of 11.5% was achieved at a D/A weight ratio of 1:1. For the devices without extra treatments, compared to the PBDB-T:ITIC-based PSCs [22], the PM6:IT-4F-based PSCs display a similar V_{oc} due to the coordinated deep-shifted HOMO levels of PM6 and IT-4F, a significantly increased J_{sc} from 16.2 to 19.4 mA cm^{-2} due to the enhanced optical absorption of the PM6:IT-4F blend. Notably, the PCE of 11.5% is among the highest values reported in the literature to date for the PSCs without extra treatments.

Subsequently, the active layer morphology was optimized to improve the device performance by adding 1,8-diiodooctane (DIO) as solvent additive and then thermal annealing (TA). The *J-V* and external quantum efficiency (EQE) curves of the PSCs under different fabrication conditions are shown in Figure 2(a, b) and Figure S2, and detailed photovoltaic parameters are summarized in Table 1 and Table S2. With the blend film processed with 0.75% DIO and TA at 100 °C for 20 min, the PSCs showed an obvious increased J_{sc} from 19.4 to 22.2 mA cm^{-2} and significantly improved FF from 66.7% to 72.5%, while the V_{oc} was slightly decreased to 0.84 V. As a result, the champion PSC achieves a PCE of up to 13.5%. Compared with the PBDB-T:ITIC-based PSCs, despite of the decreased V_{oc} from 0.90 to 0.84 V, the PM6:IT-4F-based PSCs show significantly increased J_{sc} from 16.81 to 22.2 mA cm^{-2}. Moreover, the optimal device possesses a low E_{loss} (which is defined as $E_g^{opt} - eV_{oc}$) of ca. 0.65 eV due to the small E_g^{opt} (1.49 eV) of the IT-4F film, which is close to the empirical threshold of 0.6 eV. In order to cater for the roll-to-roll production on the agenda, the PM6:IT-4F-based PSCs with a large device area of 1.00 cm^2 were also fabricated and showed a PCE of up to 11.4% with a V_{oc} of 0.80 V, J_{sc} of 19.6 mA cm^{-2} and FF of 72.8% (Figure 2(c)). To our best knowledge, the PCE of 11.4% is among the highest values reported in the literature to date for the PSCs with a device area as large as 1 cm^2.

To confirm the high J_{sc} of the PSCs, the EQE tests were carried out (Figure 2(b)). Compared to the device as-cast, the device processed with DIO and TA shows significant broadening of the EQE response range due to the increased crystallinity of IT-4F in the active layer, which agrees that the active layer possesses the red-shifted UV-Vis absorption spectra of ca. 25 nm (Figure S3). In addition, the device optimized by DIO and TA exhibited increased EQE response values in the region of 350–830 nm and has a higher max-

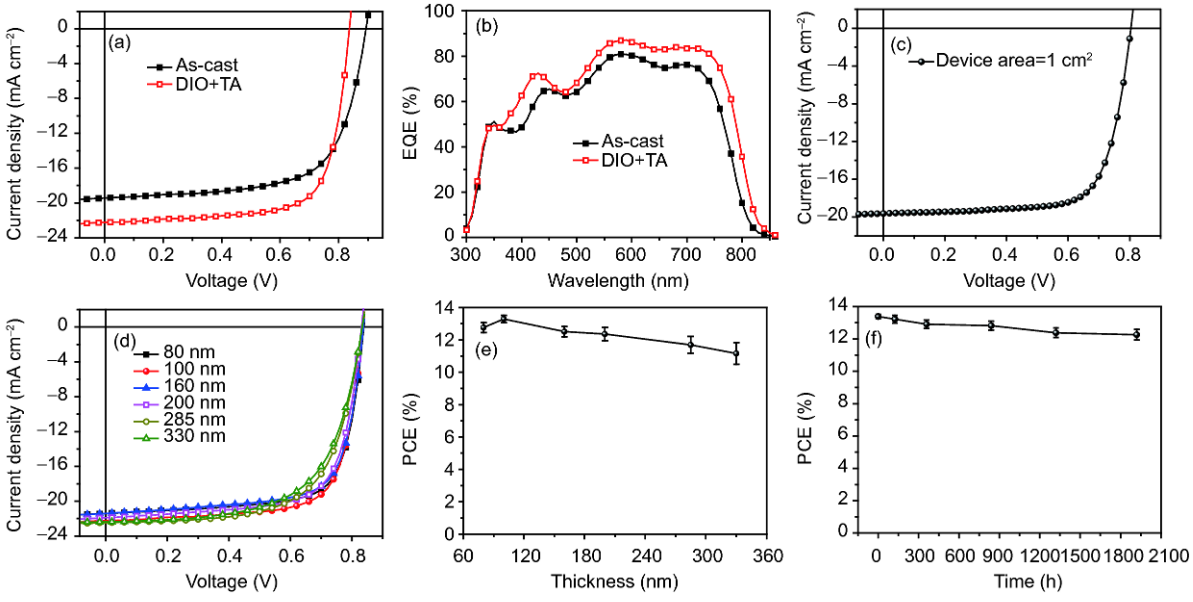

Figure 2 (a) The *J-V* and (b) EQE plots of the PSCs based on PM6:IT-4F (1:1, *w*/*w*) with different fabrication conditions. (c, d) The *J-V* plots of the PSCs processed by DIO and thermal annealing (TA) (c) with a large device area of 1 cm^2 and (d) with different active layer thicknesses. (e) PCE versus active layer thickness of the PSCs processed by DIO and TA. (f) Storage stability of the PSCs (color online).

Table 1 Photovoltaic performance date of the PSCs based on PM6:IT-4F (1:1, *w*/*w*)

PM6:IT-4F	V_{oc} (V)	J_{sc} [a] (mA cm^{-2})	FF (%)	PCE [b] (%)
As-cast	0.89	19.4 (18.5)	66.7	11.5 (11.1)
DIO [c] + TA [d]	0.84	22.2 (21.1)	72.5	13.5 (13.2)

a) The integral J_{sc} in parentheses from the EQE curves; b) the average PCEs in parentheses from 30 devices; c) with 0.75% DIO; d) with TA at 100 °C for 20 min;

imum EQE value of ca. 84% at 590 nm in comparison with the device as-cast (ca. 81% at 581 nm). Notably, the devices show the high EQE values in the absorption region belonging to IT-4F (ca. 650–830 nm), indicating that the photons absorbed by IT-4F can be efficiently converted to electrons despite only a small ΔE_{HOMO} of 0.19 eV in PM6/IT-4F pair, which corresponds well to the high photoluminescence (PL) quenching efficiency (Figure S6). The error between the integral J_{sc} and the measured J_{sc} values is less than 5%.

In addition to high efficiency and large device area, high active layer thickness tolerance is also important for the roll-to-roll device production in future. Here, the PSC devices with different active layer thicknesses of 80–330 nm were fabricated to probe the effect of thickness on the device performance (Figure 2(d) and Table S3). With increasing active layer thickness, the PSCs show little changed V_{oc}, small fluctuations of J_{sc} and decreased FF. At the thickness range of 80–285 nm, the PSCs showed PCEs of over 12% (Figure 2(e)), which is crucial for the large scale roll-to-roll fabrication of high-performance PSCs. Notably, even though the active layer thickness is up to 330 nm, the PSC still shows a PCE of up to 11.7%, which is the highest value reported in the devices with the active layer thickness over 300 nm.

High device stability is a necessary prerequisite for practical applications of PSCs. Here, we have tested the storage stability, thermal stability and light stability of the PSC devices. After 1920 h of storage in the N_2-filled glovebox, the PSCs still gain a PCE of up to 12.0% (Figure 2(f) and Table S4), indicating that the devices possess high long-term storage stability. Then, the devices annealed at a typical high temperature of 100 °C for 250 min in the N_2-filled glovebox still remained a superior PCE of 12.4% (Figure S4 and Table S5). Moreover, after continuous illumination for 300 min under AM 1.5G, 100 mW cm^{-2}, the PSCs also remained a PCE of over 10% (Figure S5 and Table S6). The above results imply that the PSC devices have good stability.

The exciton dissociation and charge extraction processes are probed by measuring the plots of photocurrent (J_{ph}) versus effective voltage (V_{eff}) of the devices (Figure 3(a)) [14,18]. The parameter definitions and calculation methods are described in detail in Supporting Information online. Under the short-circuit and maximum power output conditions, the exciton dissociation probabilities $P(E, T)$ were calculated to be 85.1% and 97.4%, 89.4% and 97.8% for the devices based on PM6:IT-4F blends as-cast, and with DIO and TA treatments respectively, implying that the PSCs possess an efficient exciton dissociation and charge extraction processes, especially in PSCs processed by DIO and TA. In order to study the charge recombination mechanism in PSCs, the relationship of V_{oc} with light intensity (P) was probed (Figure 3(b)) [22,38]. The slope of V_{oc} versus ln$P$ at k_BT/q suggests that the device only has bimolecular recombination, while the slope of 2 k_BT/q means that the trap-assisted recombination dominates in the recombination mechanisms of device (where T, k_B and q are the Kelvin temperature, Boltzmann constant and elementary charge, respectively). The device processed by DIO and TA (1.20 k_BT/q) displays a smaller slope compared to the device as-cast (1.37 k_BT/q), which implies that the device processed by DIO and TA has fewer trap-assisted recombination. Moreover, the dependence of J_{ph} under different P was defined as $J_{ph} \propto P^S$, and studied to further probe the charge recombination process in PSCs (Figure 3(c)). S values close to 1 indicate that the devices possess weak bimolecular recombination [14,61]. For the devices based on PM6:IT-4F blends as-cast, and with DIO and TA, the S values of the fitted lines in logarithmic coordinates are 0.990 and 0.999 respectively, which means that the device processed by DIO and TA has less bimolecular recombination.

PL quenching efficiency of the PM6:IT-4F blends compared to their pure films were also measured to probe the

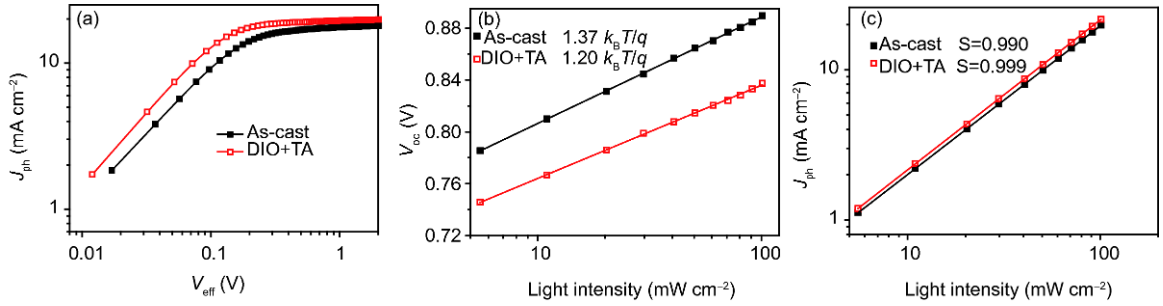

Figure 3 (a) The J_{ph} versus V_{eff}; (b) the V_{oc} and (c) the J_{ph} versus light intensity of the PM6:IT-4F (1:1, *w*/*w*)-based PSCs with different fabrication conditions (color online).

exciton dissociation and charge transport processes (Figure S6). All blend films showed a high PL quenching efficiency of more than 90%, implying that all devices possess highly efficient photo-induced exciton dissociation and charge transport processes, especially in device processed by DIO and TA, which agrees with the higher EQE and J_{sc} values of the related PSCs.

The molecular packing patterns of the blend films were measured by grazing incidence X-ray diffraction (GIXD) method as shown in Figure 4(a–d). It is seen that neat IT-4F film showed a weak structure order. No well-defined diffraction peaks can be recorded. Neat PM6 film showed a broad (100) diffraction peak in in-plane (IP) direction at 0.30 $Å^{-1}$ with a crystal coherence length (CCL) of 6.83 nm. The π-π stacking peak is more obvious in out-of-plane (OOP) direction at 1.66 $Å^{-1}$, and thus PM6 adopted a face-on orientation. As-casted blend film showed a strong polymer diffraction features. And the (100) diffraction peak of PM6 became sharper. The CCL of 10.10 nm was seen. A π-π stacking peak was recorded at 1.68 $Å^{-1}$. When DIO additive and TA treatments were used to process blend film, elevated crystallization was seen. The (100) diffraction peak area of PM6 nearly doubled comparing to the as-casted blend film, with a CCL is 13.45 nm. The corresponding π-π stacking diffraction in OOP direction shifted to 1.71 $Å^{-1}$ and showed a stronger peak, indicating a tighter packing of PM6 or crystallization of IT-4F at a higher angle comparing to the π-π stacking diffraction of neat PM6 film. The above results indicate interested properties of this blend film. Although it is commonly seen that the similar chemical structure of donor polymer and *n*-OS acceptor often leads to intimate mixing, IT-4F in this case helped boosting the crystalline order of PM6. The DIO and TA processing further improved the structure order of PM6 in blend films. Thus, improved hole-mobility is expected. The hole/electron mobilities (μ_h/μ_e) are measured using the space charge limited current method (Figure S7). The μ_h/μ_e were $3.42/2.38\times10^{-4}$ and $9.76/7.15\times10^{-4}$ cm^2 V^{-1} s^{-1} for the devices based on the blend films as-cast, and with DIO and TA, respectively. The relatively high μ_h/μ_e values and low μ_h/μ_e ratios imply more effective and balanced charge transport in the blend films with DIO and TA treatments, and thus a high J_{sc} and FF can be achieved for the PSCs. Notably, compared to the PM6:ITIC-based devices ($6.08/5.05\times10^{-4}$ cm^2 V^{-1} s^{-1}) [60], the devices based on PM6:IT-4F possess higher μ_h/μ_e values, which is well consistent with the fact that the device based on PM6:IT-4F has higher FF value.

Phase separation of blend films was studied using resonant soft X-ray scattering (RSoXS) at 285 eV photon energy [62]. As shown in Figure 4(e), as-casted blend film showed a weak scattering profile, which indicates a weak phase separation. DIO and TA processing blend film showed a higher scattering intensity with a broad hump and center at 0.0085 $Å^{-1}$. The average center to center distance is ≈74 nm, which means a statistics average domain size of ≈37 nm. Such a phase separation length scale is larger than the lamellae stacking of PM6 in IP direction, and thus demixing induced phase separation dominates the morphology. When improved polymer crystallization can improve hole-mobility, increased extend of phase separation results in purer acceptor-rich domain. And thus improved electron-mobility is expected. Higher mobility for both hole and electron reduces series resistance of the PSCs, and thus increased FF was seen. Moreover, efficient charge transport and collection improves J_{sc}. These results agreed quite well with our device characterizations.

The surface and bulk morphologies of PM6:IT-4F films were further studied. For atomic force microscopy (AFM)

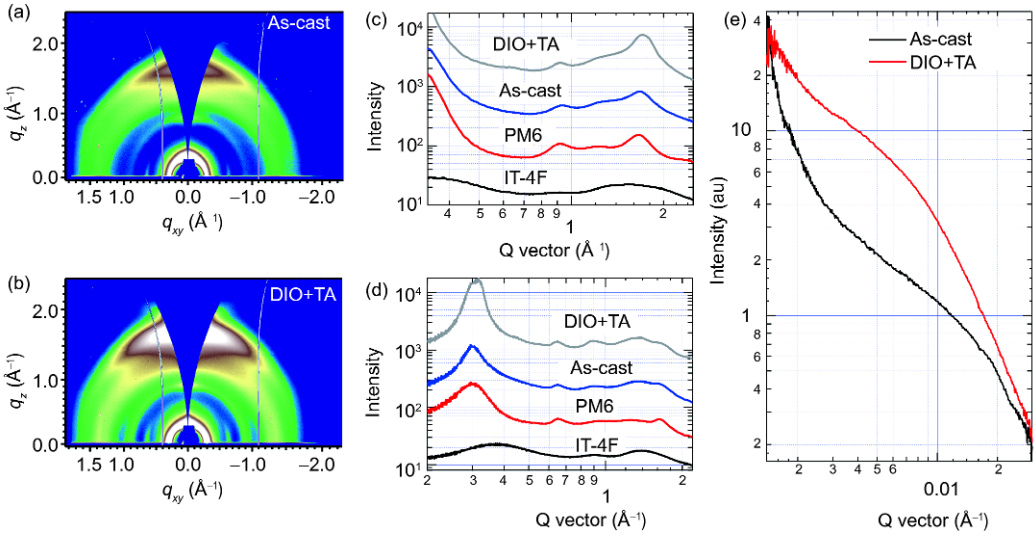

Figure 4 (a, b) 2D-GIXD pattern of the PM6:IT-4F films processed from different conditions; (c) OOP and (d) IP line-cut profiles of 2D-GIXD results; (e) RSoXS profiles of the PM6:IT-4F films processed from different conditions (color online).

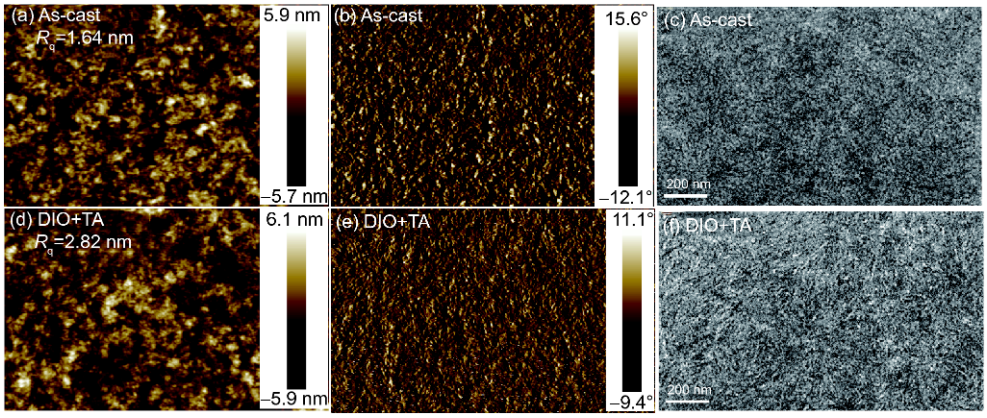

Figure 5 The AFM (5 μm×3 μm) and TEM images of the PM6:IT-4F blend films (a–c) as-cast, and (d–f) with DIO and TA (color online). (a, b, d, e) AFM; (c, f) TEM.

images (Figure 5(a, b, d, e)), the blend as-cast showed a smooth surface with a a root mean square roughness (R_q) value of 1.64 nm, while the blend processed by DIO and TA displayed a rough surface due to increased material crystallization and phase separation [14,15]. The phase image became sharper when DIO and TA treatments are used, indicating enhanced phase separation, which agrees well with GIXD and RSoXS tests. For transmission electron microscopy (TEM) images (Figure 5(c, f)), the blend as-cast also showed a weak phase separation. The blend processed by DIO and TA displayed suitable phase separation and a fibril texture with size of ca. 20 nm, which facilitates exciton separation and charge transport and hence improved the J_{sc} and FF values in PSCs.

3 Conclusions

We developed a high performance PSC based on both fluorinated polymer donor PM6 and *n*-OS acceptor IT-4F. The PM6:IT-4F blend possesses the wide and complementary absorption spectra from ca. 300 to 830 nm and well-matched energy levels. Furthermore, the strong crystallinity of PM6 is beneficial to form favorable blend morphology and hence to suppress recombination in devices. The optimal PM6:IT-4F-based PSC achieved an impressive PCE of 13.5%, which is among the highest values in the literature for PSCs to date. Furthermore, a PCE of 12.2% was remained with the active layer thickness of up to 285 nm and a high PCE of 11.4% was also obtained with a large device area of 1 cm^2. In addition, the devices also showed good storage, thermal and illumination stabilities with respect to the efficiency. The above results indicate that the PM6:IT-4F blend is an ideal candidate for the large scale roll-to-roll production of efficient PSCs in the future.

Acknowledgements This work was supported by the National Natural Science Foundation of China (51422306, 51503135, 51573120, 91633301), and Jiangsu Provincial Natural Science Foundation (BK20150332). T. P. Russell was supported by the U.S. Office of Naval Research (N00014-15-1-2244). Portions of this research were carried out at beamline 7.3.3 and 11.0.1.2 at the Advanced Light Source, Molecular Foundry, and National Center for Electron Microscopy, Lawrence Berkeley National Laboratory, which was supported by the DOE, Office of Science, and Office of Basic Energy Sciences.

Conflict of interest The authors declare that they have no conflict of interest.

Supporting information The supporting information is available online at http://chem.scichina.com and http://link.springer.com/journal/11426. The supporting materials are published as submitted, without typesetting or editing. The responsibility for scientific accuracy and content remains entirely with the authors.

1 Stoltzfus DM, Donaghey JE, Armin A, Shaw PE, Burn PL, Meredith P. *Chem Rev*, 2016, 116: 12920–12955
2 Hwang YJ, Li H, Courtright BAE, Subramaniyan S, Jenekhe SA. *Adv Mater*, 2016, 28: 124–131
3 Kwon OK, Park JH, Kim DW, Park SK, Park SY. *Adv Mater*, 2015, 27: 1951–1956
4 Wu Q, Zhao D, Schneider AM, Chen W, Yu L. *J Am Chem Soc*, 2016, 138: 7248–7251
5 Long X, Ding Z, Dou C, Zhang J, Liu J, Wang L. *Adv Mater*, 2016, 28: 6504–6508
6 Zhou N, Dudnik AS, Li TING, Manley EF, Aldrich TJ, Guo P, Liao HC, Chen Z, Chen LX, Chang RPH, Facchetti A, Olvera de la Cruz M, Marks TJ. *J Am Chem Soc*, 2016, 138: 1240–1251
7 Baran D, Ashraf RS, Hanifi DA, Abdelsamie M, Gasparini N, Röhr JA, Holliday S, Wadsworth A, Lockett S, Neophytou M, Emmott CJM, Nelson J, Brabec CJ, Amassian A, Salleo A, Kirchartz T, Durrant JR, McCulloch I. *Nat Mater*, 2017, 16: 363–369
8 Li Z, Xu X, Zhang W, Meng X, Ma W, Yartsev A, Inganäs O, Andersson MR, Janssen RAJ, Wang E. *J Am Chem Soc*, 2016, 138: 10935–10944
9 Lee C, Kang H, Lee W, Kim T, Kim KH, Woo HY, Wang C, Kim BJ. *Adv Mater*, 2015, 27: 2466–2471
10 Jia J, Zheng N, Wang Z, Huang Y, Duan C, Huang F, Cao Y. *Sci China Chem*, 2017, 60: 1458–1467
11 Su W, Fan Q, Guo X, Guo B, Li W, Zhang Y, Zhang M, Li Y. *J Mater Chem A*, 2016, 4: 14752–14760
12 Zhang S, Yang L, Liu D, He C, Zhang J, Zhang Y, Hou J. *Sci China Chem*, 2017, 60: 1340–1348

13 Fan Q, Su W, Guo X, Wang Y, Chen J, Ye C, Zhang M, Li Y. *J Mater Chem A*, 2017, 5: 9204–9209
14 Guo B, Li W, Guo X, Meng X, Ma W, Zhang M, Li Y. *Adv Mater*, 2017, 29: 1702291
15 Fan Q, Wang Y, Zhang M, Wu B, Guo X, Jiang Y, Li W, Guo B, Ye C, Su W, Fang J, Ou X, Liu F, Wei Z, Sum TC, Russell TP, Li Y. *Adv Mater*, 2017, 116: 1704546
16 Cui Y, Yao H, Yang C, Zhang S, Hou J. *Acta Polym Sin*, 2017, doi: 10.11777/j.issn1000-3304.2018.17297
17 Xu X, Yu T, Bi Z, Ma W, Li Y, Peng Q. *Adv Mater*, 2017, 45: 1703973
18 Dai S, Zhao F, Zhang Q, Lau TK, Li T, Liu K, Ling Q, Wang C, Lu X, You W, Zhan X. *J Am Chem Soc*, 2017, 139: 1336–1343
19 Zhao F, Dai S, Wu Y, Zhang Q, Wang J, Jiang L, Ling Q, Wei Z, Ma W, You W, Wang C, Zhan X. *Adv Mater*, 2017, 29: 1700144
20 Chen S, Liu Y, Zhang L, Chow PCY, Wang Z, Zhang G, Ma W, Yan H. *J Am Chem Soc*, 2017, 139: 6298–6301
21 Li W, Yan D, Liu W, Chen J, Xu W, Zhan C, Yao J. *Sol RRL*, 2017, 1: 1700014
22 Zhao W, Qian D, Zhang S, Li S, Inganäs O, Gao F, Hou J. *Adv Mater*, 2016, 28: 4734–4739
23 Zheng Z, Awartani OM, Gautam B, Liu D, Qin Y, Li W, Bataller A, Gundogdu K, Ade H, Hou J. *Adv Mater*, 2017, 29: 1604241
24 Bin H, Gao L, Zhang ZG, Yang Y, Zhang Y, Zhang C, Chen S, Xue L, Yang C, Xiao M, Li Y. *Nat Commun*, 2016, 7: 13651
25 Yu T, Xu X, Zhang G, Wan J, Li Y, Peng Q. *Adv Funct Mater*, 2017, 27: 1701491
26 Zhao W, Li S, Yao H, Zhang S, Zhang Y, Yang B, Hou J. *J Am Chem Soc*, 2017, 139: 7148–7151
27 Xie D, Liu T, Gao W, Zhong C, Huo L, Luo Z, Wu K, Xiong W, Liu F, Sun Y, Yang C. *Sol RRL*, 2017, 1: 1700044
28 Lin Y, Zhao F, Wu Y, Chen K, Xia Y, Li G, Prasad SKK, Zhu J, Huo L, Bin H, Zhang ZG, Guo X, Zhang M, Sun Y, Gao F, Wei Z, Ma W, Wang C, Hodgkiss J, Bo Z, Inganäs O, Li Y, Zhan X. *Adv Mater*, 2017, 29: 1604155
29 Su W, Fan Q, Guo X, Meng X, Bi Z, Ma W, Zhang M, Li Y. *Nano Energy*, 2017, 38: 510–517
30 Zhao W, Zhang S, Hou J. *Sci China Chem*, 2016, 59: 1574–1582
31 Lin Y, Wang J, Zhang ZG, Bai H, Li Y, Zhu D, Zhan X. *Adv Mater*, 2015, 27: 1170–1174
32 Li S, Ye L, Zhao W, Zhang S, Mukherjee S, Ade H, Hou J. *Adv Mater*, 2016, 28: 9423–9429
33 Li Y, Zhong L, Gautam B, Bin HJ, Lin JD, Wu FP, Zhang Z, Jiang ZQ, Zhang ZG, Gundogdu K, Li Y, Liao LS. *Energy Environ Sci*, 2017, 10: 1610–1620
34 Yao H, Cui Y, Yu R, Gao B, Zhang H, Hou J. *Angew Chem Int Ed*, 2017, 56: 3045–3049
35 Liu Y, Zhang Z, Feng S, Li M, Wu L, Hou R, Xu X, Chen X, Bo Z. *J Am Chem Soc*, 2017, 139: 3356–3359
36 Liu F, Zhou Z, Zhang C, Vergote T, Fan H, Liu F, Zhu X. *J Am Chem Soc*, 2016, 138: 15523–15526
37 Fan B, Zhang K, Jiang XF, Ying L, Huang F, Cao Y. *Adv Mater*, 2017, 29: 1606396
38 Fan Q, Xu Z, Guo X, Meng X, Li W, Su W, Ou X, Ma W, Zhang M, Li Y. *Nano Energy*, 2017, 40: 20–26
39 Kan B, Feng H, Wan X, Liu F, Ke X, Wang Y, Wang Y, Zhang H, Li C, Hou J, Chen Y. *J Am Chem Soc*, 2017, 139: 4929–4934
40 Zhang M, Guo X, Zhang S, Hou J. *Adv Mater*, 2014, 26: 1118–1123
41 Zhang M, Guo X, Ma W, Ade H, Hou J. *Adv Mater*, 2015, 27: 4655–4660
42 Bin H, Zhong L, Zhang ZG, Gao L, Yang Y, Xue L, Zhang J, Zhang Z, Li Y. *Sci China Chem*, 2016, 59: 1317–1322
43 Fan Q, Su W, Meng X, Guo X, Li G, Ma W, Zhang M, Li Y. *Sol RRL*, 2017, 1: 1700020
44 Liu Y, Zhao J, Li Z, Mu C, Ma W, Hu H, Jiang K, Lin H, Ade H, Yan H. *Nat Commun*, 2014, 5: 5293
45 Jo JW, Jung JW, Jung EH, Ahn H, Shin TJ, Jo WH. *Energy Environ Sci*, 2015, 8: 2427–2434
46 Deng Y, Liu J, Wang J, Liu L, Li W, Tian H, Zhang X, Xie Z, Geng Y, Wang F. *Adv Mater*, 2014, 26: 471–476
47 Li W, Albrecht S, Yang L, Roland S, Tumbleston JR, McAfee T, Yan L, Kelly MA, Ade H, Neher D, You W. *J Am Chem Soc*, 2014, 136: 15566–15576
48 Yan T, Bin H, Yang Y, Xue L, Zhang ZG, Li Y. *Sci China Chem*, 2017, 60: 537–544
49 Fan Q, Su W, Guo X, Guo B, Li W, Zhang Y, Wang K, Zhang M, Li Y. *Adv Energy Mater*, 2016, 6: 1600430
50 Fan Q, Su W, Guo X, Zhang X, Xu Z, Guo B, Jiang L, Zhang M, Li Y. *J Mater Chem A*, 2017, 5: 5106–5114
51 Zhang Q, Kelly MA, Bauer N, You W. *Acc Chem Res*, 2017, 50: 2401–2409
52 Fan Q, Jiang H, Liu Y, Su W, Tan H, Wang Y, Yang R, Zhu W. *J Mater Chem C*, 2016, 4: 2606–2613
53 Jung JW, Jo JW, Chueh CC, Liu F, Jo WH, Russell TP, Jen AKY. *Adv Mater*, 2015, 27: 3310–3317
54 Jheng JF, Lai YY, Wu JS, Chao YH, Wang CL, Hsu CS. *Adv Mater*, 2013, 25: 2445–2451
55 Bronstein H, Frost JM, Hadipour A, Kim Y, Nielsen CB, Ashraf RS, Rand BP, Watkins S, McCulloch I. *Chem Mater*, 2013, 25: 277–285
56 Kawashima K, Fukuhara T, Suda Y, Suzuki Y, Koganezawa T, Yoshida H, Ohkita H, Osaka I, Takimiya K. *J Am Chem Soc*, 2016, 138: 10265–10275
57 Jo JW, Jung JW, Wang HW, Kim P, Russell TP, Jo WH. *Chem Mater*, 2014, 26: 4214–4220
58 Yang F, Li C, Lai W, Zhang A, Huang H, Li W. *Mater Chem Front*, 2017, 1: 1389–1395
59 Qian D, Ye L, Zhang M, Liang Y, Li L, Huang Y, Guo X, Zhang S, Tan Z, Hou J. *Macromolecules*, 2012, 45: 9611–9617
60 Wang Y, Fan Q, Guo X, Li W, Guo B, Su W, Ou X, Zhang M. *J Mater Chem A*, 2017, 5: 22180–22185
61 Xu Z, Fan Q, Meng X, Guo X, Su W, Ma W, Zhang M, Li Y. *Chem Mater*, 2017, 29: 4811–4818
62 Swaraj S, Wang C, Yan H, Watts B, Luning J, McNeill CR, Ade H. *Nano Lett*, 2010, 10: 2863–2869